Ab initio electronic structure study for TTF-TCNQ under uniaxial compression

Shoji Ishibashi,[1] Tamotsu Hashimoto,[1] Masanori Kohyama,[1,2] and Kiyoyuki Terakura[1]
[1]*Research Institute for Computational Sciences (RICS), National Institute of Advanced Industrial Science and Technology (AIST), Central 2, 1-1-1 Umezono, Tsukuba, Ibaraki 305-8568, Japan*
[2]*Special Division of Green Life Technology, National Institute of Advanced Industrial Science and Technology (AIST), 1-8-31 Midorigaoka, Ikeda, Osaka 563-8577, Japan*
(Received 9 July 2003; revised manuscript received 15 January 2004; published 16 April 2004)

We have investigated the electronic structure of TTF-TCNQ under uniaxial compression with *ab initio* plane-wave pseudopotential calculations within the local-density approximation and generalized gradient approximation. Depending on the compression direction, the constituent molecules are deformed in different ways. Along with these structural deformations, quasi-one-dimensional Fermi surfaces show dramatic changes in their shapes and sizes.

DOI: 10.1103/PhysRevB.69.155111 PACS number(s): 71.20.Rv, 71.18.+y

I. INTRODUCTION

The organic compound tetrathiofulvalene-tetracyanoquinodimethane[1,2] (TTF-TCNQ: TTF$=C_6H_4S_4$, TCNQ $=C_{12}H_4N_4$) has a monoclinic crystal structure (space group $P2_1/c$) where cations (TTF) and anions (TCNQ) form separate columns along the *b* axis.[3,4] Quasi-one-dimensional metallic conductivity along this direction is observed above 58 K.[2] A charge transfer from TTF to TCNQ is the source of the conductivity. At room temperature, 0.55 electrons/molecule transfer from TTF to TCNQ.[5] Below 150 K, the charge-transfer value is 0.59 electrons/molecule.[5] The charge transfer is not only a function of temperature but also a function of pressure. Megtert *et al.*[6] reported an increase of the charge transfer to 0.616 electrons/molecule at 5 kbar.

As for theoretical studies of the electronic band structure of TTF-TCNQ, first, band parameters based on the tight-binding approximation were estimated through molecular-orbital calculations.[7,8] Shitzkovsky *et al.*[9] investigated the Fermi-surface shape with various band parameters and showed the importance of the intercolumn coupling. *Ab initio* calculations were made also though early ones[10,11] were inconsistent with the previous tight-binding calculations and the experimental results. As a known fact, before the first success for the DCNQI (dicyanoquinonediimine) systems,[12] *ab initio* calculations had not well succeeded in describing electronic structures of molecular conductors. These days, the situation is different.

We reported *ab initio* electronic structure calculations for TTF-TCNQ and TSeF-TCNQ (TSeF, tetraselenafulvalene) with the experimentally obtained crystal structures.[13,14] Systematic comparisons of the obtained electronic structures were made between the results obtained with the local-density approximation (LDA) and the generalized gradient approximation (GGA), or among the results for the room-temperature (RT) structure of TTF-TCNQ, the 100 K structure of TTF-TCNQ, and the RT structure of TSeF-TCNQ. For the same structure, the difference between the LDA and GGA results is marginal. The lattice-parameter decrease with temperature decreasing from RT to 100 K causes an increase of the bandwidth. The substitution of Se for S is reasonably reflected on the obtained band structures. The bands derived from the highest occupied molecular orbital (HOMO) of TSeF have larger bandwidths than those of the TTF-HOMO bands. The widths of the bands derived from the lowest unoccupied molecular orbital (LUMO) of TCNQ show slight decreases reflecting small increase of the lattice parameters with the substitution. Although the charge transfer between TTF and TCNQ is somewhat overestimated as 0.7 electrons/molecule, most results are reasonable in light of existing experimental results. For example, the obtained data for all valence electrons were utilized to simulate Compton scattering profiles as well as positron annihilation spectra and gave successful results.[15–17] Later calculations of the TTF-TCNQ band structure with other *ab initio* methods[18,19] are in good agreement with our previous results[14] mentioned above.

Recently, Kagoshima *et al.*[20] have attempted to control electronic properties of organic conductors by hydrostatic and uniaxial compression. The application of the uniaxial compression is a novel technique and has an advantage compared with the conventional uniaxial stress techniques. The uniaxial compression brings purely reduction of the lattice along a desired direction, while the uniaxial stress induces expansion of the lattice in the plane perpendicular to the stress direction due to the Poisson effect. The uniaxial compression technique enables us to make well-screened changes for the intermolecular distance and the electronic properties of the organic conductors. Note, however, under compression, experimental determination of the atomic positions is difficult or sometimes impossible. For such a case, theoretical supports become crucial.

In the present work, atomic positions were optimized with an *ab initio* molecular-dynamics technique on the experimentally determined unit cell. The results were compared with the experimental results in order to examine the accuracy of the computational technique. Next, we investigated effects of uniaxial compression along three different crystallographic axes *a*, *b*, and *c** (reciprocal-lattice vector) on the electronic structure of TTF-TCNQ through *ab initio* band calculations with optimizing the atomic positions. As mentioned above, TTF-TCNQ has a very anisotropic electronic structure and subtle balance between intracolumn and intercolumn couplings determineing the shape of the Fermi surface. Compression along different directions is expected to

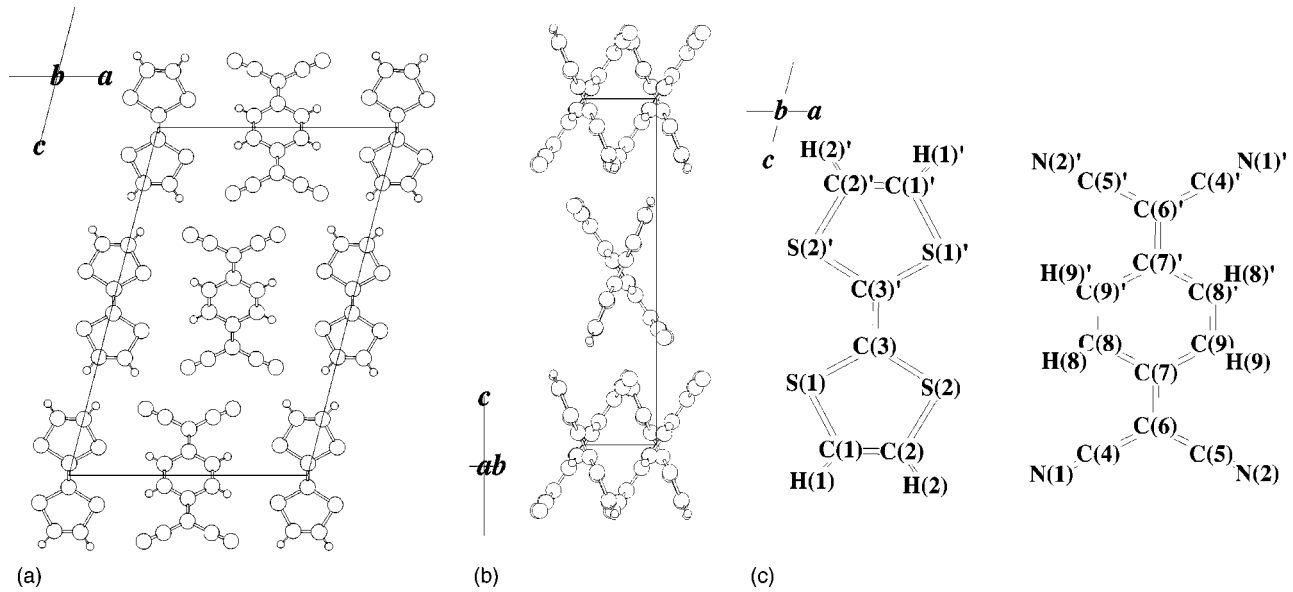

FIG. 1. Crystal structure of TTF-TCNQ (Refs. 3 and 4), (a) view in the ac plane, (b) view in the bc plane, and (c) constituent atoms.

result in different electronic structures.

II. COMPUTATIONAL DETAILS

The present calculations are based on the plane-wave norm-conserving pseudopotential method.[21] We used pseudopotentials proposed by Troullier and Martins[22] with the separable approximation[23] and the partial core correction.[24] As for the exchange and correlation energy for electrons, we have tested both LDA (Refs. 25 and 26) and GGA.[27] To obtain the final converged wave function, the preconditioned conjugate gradient method[28] modified by Bylander *et al.*[29] with the charge mixing scheme by Kerker,[30] which has been shown to be suitable for large metallic systems,[31] was used together with the Gaussian smearing technique.[32] The total energy and Hellmann-Feynman forces were obtained according to expressions in Ref. 33

We used the plane-wave cutoff energy $E_{cut}^{PW}=60$ Ry. A good convergence was confirmed by comparing the results with those obtained with $E_{cut}^{PW}=65$ Ry for some cases. Sixteen $\boldsymbol{k}$ points were used in the irreducible zone (1/4 of the Brillouin zone). In our previous work, we confirmed that even eight points were enough to obtain good convergence.[14] In quenched molecular dynamics, one time step was 1–1.5 fs. The criterion of the convergence is less than 10^{-4} Ry/a.u. for atomic forces.

For the unit cell of 100 K structure[4] as well as cells compressed by 10% along three directions, atomic positions were fully relaxed and electronic band dispersions were calculated.

III. RESULTS AND DISCUSSION

Figure 1 represents the crystallographic view of TTF-TCNQ [panels (a) and (b)] and the atomic species of TTF and TCNQ [panel (c)].[3,4] Before showing uniaxial-compression effects, we would like to mention the results of atomic-position optimization on the unit cell experimentally determined at 100 K.[4] The resultant bond lengths and bond angles are listed in Tables I and II together with the experimental results. As for bond length, generally, the LDA values are slightly shorter than the corresponding GGA ones. For LDA, the lengths for the single bonds [S(1)-C(1), S(1)-C(3), S(2)-C(2), S(2)-C(3), C(4)-C(6), C(5)-C(6), C(7)-C(8), C(7)-C(9)] are underestimated while those for the double bonds [C(1)-C(2), C(3)-C(3)′, C(6)-C(7), C(8)-C(9)′] and the triple bonds [N(1)-C(4), N(2)-C(5)] are overestimated. The GGA results show similar tendency, but the values for the single bonds are much better than those for LDA. Since it is well known that experimental C-H bond lengths are systematically underestimated due to asymmetric charge distribution around H atoms, the results involving H atoms are not listed in tables. For reference, the average C-H bond length is 0.928 Å while those for LDA and GGA are 1.097 Å and 1.096 Å, respectively. As for bond angle, both LDA and GGA give very good results for TTF. Differences between the experimental and the calculated values are comparable to experimental errors (typically 0.2°). In contrast, the agreement with the experiment is worse for TCNQ, especially at one cyano group [N(1)-C(4)-C(6)]. Larger thermal motion of the cyano groups[4] is a possible origin of the difference. Although the maximum difference values of 0.029 Å and 2.1° are one order of magnitude larger than the experimental errors (typically 0.003 Å and 0.2°), they are still acceptably small for theoretical prediction of crystal structures.

Under 10% compression, it is naturally thought that molecules are deformed. As for the bond length, however, the change is very small regardless of compression direction, the largest change being only 0.01 Å. In contrast, bond angles change in different ways depending on the compression direction. In Table III, calculated bond angles for three compressed lattices are compared with those for the uncompressed one. The difference between the LDA results and the GGA results is marginal. For the compression along a, the

TABLE I. Comparison of bond lengths. ''EXP'' represents experimental values at 100 K reported by Blessing and Coppens (Ref. 4). The numbers in parentheses are estimated standard deviations for the last digits (Ref. 4). The present results are given in the columns labeled LDA and GGA. Their deviations from the experimental values are given as Δ_{LDA},Δ_{GGA}. Some of them do not exactly correspond with the difference between the two values because of round-off error.

	EXP (Å)	LDA (Å)	Δ_{LDA} (Å)	GGA (Å)	Δ_{GGA} (Å)
TTF					
S(1)-C(1)	1.734(3)	1.717	−0.017	1.732	−0.002
S(1)-C(3)	1.746(2)	1.726	−0.020	1.743	−0.003
S(2)-C(2)	1.732(3)	1.716	−0.016	1.731	−0.001
S(2)-C(3)	1.738(3)	1.731	−0.007	1.747	0.009
C(1)-C(2)	1.333(3)	1.348	0.015	1.354	0.021
C(3)-C(3)′	1.365(5)	1.388	0.023	1.394	0.029
TCNQ					
N(1)-C(4)	1.149(3)	1.168	0.019	1.173	0.024
N(2)-C(5)	1.148(3)	1.169	0.021	1.174	0.026
C(4)-C(6)	1.432(3)	1.407	−0.025	1.415	−0.017
C(5)-C(6)	1.431(3)	1.405	−0.026	1.414	−0.017
C(6)-C(7)	1.395(3)	1.417	0.022	1.424	0.029
C(7)-C(8)	1.431(3)	1.422	−0.009	1.433	0.002
C(7)-C(9)	1.435(3)	1.421	−0.014	1.431	−0.004
C(8)-C(9)′	1.352(4)	1.365	0.013	1.373	0.021

angle between the cyano groups of TCNQ [C(4)-C(6)-C(5)] shows a decrease of more than 6°. For the *b* compression, the molecular shapes are not much changed. The angle N(2)-C(5)-C(6) shows a slight decrease. For the c^* compression, the angle between the cyano groups of TCNQ [C(4)-C(6)-C(5)] opens more and the cyano groups bend more [N(2)-C(5)-C(6) and N(1)-C(4)-C(6)]. The cyano-group parts of TCNQ are sensitive to cell compression. It is quite reason-

TABLE II. Comparison of bond angles. ''EXP'' represents experimental values at 100 K reported by Blessing and Coppens (Ref. 4). The numbers in parentheses are estimated standard deviations for the last digits (Ref. 4). The present results are given in the columns labeled LDA and GGA. Their deviations from the experimental values are given as Δ_{LDA},Δ_{GGA}. Some of them do not exactly correspond with the difference between the two values because of round-off error.

	EXP (deg)	LDA (deg)	Δ_{LDA} (deg)	GGA (deg)	Δ_{GGA} (deg)
TTF					
C(1)-S(1)-C(3)	94.7(1)	94.9	0.2	95.0	0.3
C(2)-S(2)-C(3)	95.2(1)	95.1	−0.1	95.3	0.1
S(1)-C(1)-C(2)	117.8(2)	117.6	−0.2	117.6	−0.2
S(2)-C(2)-C(1)	117.3(2)	117.0	−0.3	117.0	−0.3
S(1)-C(3)-S(2)	114.9(1)	115.4	0.5	115.0	0.1
S(1)-C(3)-C(3)′	121.9(2)	122.1	0.2	122.3	0.4
S(2)-C(3)-C(3)′	123.1(2)	122.5	−0.6	122.7	−0.4
TCNQ					
N(1)-C(4)-C(6)	177.3(2)	175.2	−2.1	175.2	−2.1
N(2)-C(5)-C(6)	176.7(2)	176.0	−0.7	176.5	−0.2
C(4)-C(6)-C(5)	118.0(2)	120.0	2.0	119.3	1.3
C(4)-C(6)-C(7)	120.9(2)	119.7	−1.2	119.8	−1.1
C(5)-C(6)-C(7)	121.1(2)	120.2	−0.9	120.9	−0.2
C(6)-C(7)-C(8)	121.7(2)	121.1	−0.6	121.0	−0.7
C(6)-C(7)-C(9)	121.4(2)	121.3	−0.1	121.3	−0.1
C(8)-C(7)-C(9)	116.9(2)	117.5	0.6	117.7	0.8
C(7)-C(8)-C(9)′	121.7(2)	121.2	−0.5	121.1	−0.6
C(7)-C(9)-C(8)′	121.4(2)	121.3	−0.1	121.2	−0.2

TABLE III. Comparison of bond angles for uniaxially compressed crystals. Deviations in percentage are evaluated against the calculated values for the experimental lattice listed in the LDA or GGA column of Table II.

	Δ^a_{LDA} (deg)	Δ^a_{GGA} (deg)	Δ^b_{LDA} (deg)	Δ^b_{GGA} (deg)	Δ^{c*}_{LDA} (deg)	Δ^{c*}_{GGA} (deg)
TTF						
C(1)-S(1)-C(3)	0.45	0.54	−0.15	−0.35	−1.05	−1.43
C(2)-S(2)-C(3)	0.46	0.58	−0.10	−0.32	−0.96	−1.36
S(1)-C(1)-C(2)	−0.18	−0.32	0.13	0.17	0.35	0.44
S(2)-C(2)-C(1)	−0.08	−0.01	−0.05	0.03	0.29	0.41
S(1)-C(3)-S(2)	−0.63	−0.79	0.20	0.50	1.39	1.95
S(1)-C(3)-C(3)′	0.32	0.53	−0.17	−0.29	−0.60	−0.77
S(2)-C(3)-C(3)′	0.29	0.24	−0.05	−0.23	−0.79	−1.19
TCNQ						
N(1)-C(4)-C(6)	1.11	0.62	−0.83	−0.60	−3.11	−3.41
N(2)-C(5)-C(6)	−0.73	−1.73	−1.38	−2.57	−6.10	−7.73
C(4)-C(6)-C(5)	−6.73	−6.21	0.74	1.40	3.94	4.82
C(4)-C(6)-C(7)	3.06	3.03	−0.30	−0.06	−1.30	−1.33
C(5)-C(6)-C(7)	3.67	3.21	−0.44	−1.31	−2.64	−3.46
C(6)-C(7)-C(8)	−0.02	−0.19	−0.15	0.00	−0.37	−0.40
C(6)-C(7)-C(9)	0.39	0.39	−0.24	−0.36	−0.43	−0.52
C(8)-C(7)-C(9)	−0.35	−0.18	0.31	0.30	0.81	0.93
C(7)-C(8)-C(9)′	0.25	0.22	−0.21	−0.28	−0.46	−0.55
C(7)-C(9)-C(8)′	0.07	−0.09	−0.14	−0.05	−0.35	−0.37

able from the molecular geometry. On the other hand, the molecular shape of TTF does not show remarkable changes.

In addition to the molecule deformations mentioned above, the compression causes another type of changes for the crystal structure. The angle between the normal of the TTF or TCNQ plane and the *b* axis also changes. In Table IV, resultant angle values are listed. The LDA and GGA results are very similar to each other. As for the *b* compression and the *c* compression, the observed changes of the angles are quite natural considering the relationship between the compression direction and the molecular direction. The *a* compression case is somewhat special. Only the TTF molecules are inclined more.

The band structure is thought to be modified with the compression. Figure 2 represents the GGA results for the band dispersions near the Fermi level for the above-mentioned four structures. The LDA results (not shown) are similar to the corresponding GGA ones. In order to make quantitative comparison, tight-binding parameters have been obtained by fitting the present results to a model. Six transfer integrals t^b_F, t^b_Q, t^c_F, t^c_Q, t^a_{FQ}, and ν, and the charge transfer ρ from TTF to TCNQ were adopted as fitting parameters according to Ref. 9. The suffixes *F* and *Q* represent TTF and TCNQ, respectively. t^b_F and t^b_Q represent intracolumn transfer along *b* while t^c_F and t^c_Q are intercolumn transfer between homologous columns along $b/2+c/2$. t^a_{FQ} are intercolumn transfer between heterologous columns along $a/2-b$ or $a/2+b$. ν is also intercolumn transfer between heterologous columns along $-a/2-b/2-c/2$ or $-a/2+b/2-c/2$. Further details of the fitting procedure is described in our previous paper.[14] The resultant values are listed in Table V. As for the transfer integrals along the *b* axis (t^b_F and t^b_Q) and the transferred charges ρ, their magnitudes for the LDA are slightly larger than those for the GGA. This may be due to the difference in the optimized atomic positions. Our previous results on the common atomic positions show much less difference between LDA and GGA.[14] Reflecting the differences in molecular-shape deformation and the molecular orientation, the electronic structure changes in different ways under

TABLE IV. Angles between the normal of the mean molecular plane and the *b* axis.

	Expt. lattice			10% *a*		10% *b*		10% *c**	
	EXP[a]	LDA	GGA	LDA	GGA	LDA	GGA	LDA	GGA
TTF	24.0°	22.2°	22.8°	27.2°	27.4°	19.1°	19.4°	27.9°	28.0°
TCNQ	33.8°	35.2°	33.6°	35.3°	33.8°	32.6°	31.6°	37.3°	37.0°

[a]The values given in Ref. 4 are 24.1° and 34.0° for TTF and TCNQ, respectively. Small differences with the present results would be due to round-off errors or different definitions of the mean planes.

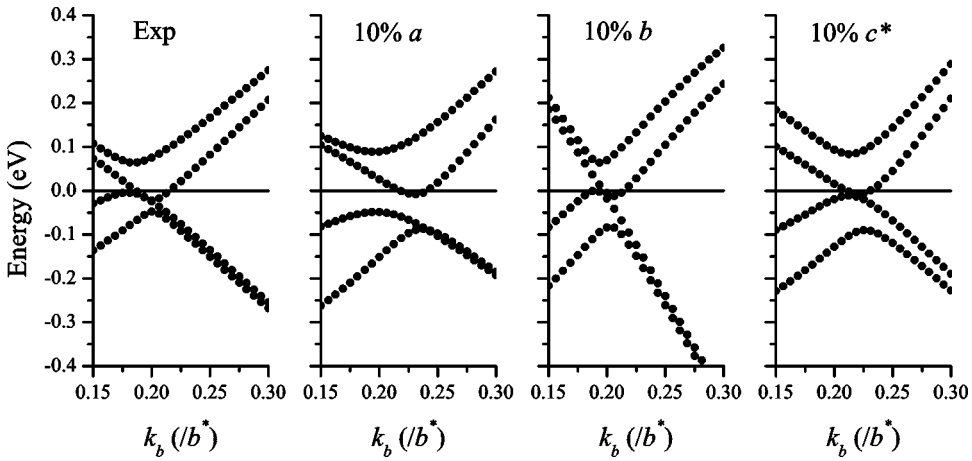

FIG. 2. Electronic band structure of TTF-TCNQ near the Fermi level calculated on the experimental unit cell and the compressed cells along the *a*, *b*, and *c** axes, respectively. The GGA results are shown.

three types of compression. For the *a* compression, a distinct change appears in the charge-transfer value. The TTF columns and the TCNQ columns are alternately arranged along the *a* axis and it is expected that the *a* compression causes an increase of the coupling between TTF and TCNQ, which is a possible origin of the increase of the charge transfer. For the LDA, the increase of coupling appears as an increase of the magnitude of t_{FQ}^a. For the GGA, there is a significant increase of the magnitude of ν. Although LDA and GGA gave similar molecular-shape changes under the *a* compression as described above, the effect appears in a different way implying that these parameters, which relate to transfer along the *a* direction, are very sensitive to subtle changes of the crystal structure. In addition, the above-mentioned deformation of TCNQ may affect the energy level of the TCNQ-LUMO-derived bands. Another noticeable change is the decrease of t_F^b. This would be ascribed to the incline of the TTF molecules. For the *b* compression, quite naturally, the magnitudes of the transfer integrals along the *b* axis (t_F^b and t_Q^b) increase significantly. The change of the charge transfer is relatively small. For the *c* compression, the magnitudes of the transfer integrals t_F^c and t_Q^c increase. The charge transfer also increases. Similar to the *a*-compression case, the increase of coupling between TTF and TCNQ and/or the deformation of the cyano groups could be an origin of the charge-transfer increase. Previously, the increase of the charge transfer under hydrostatic pressure was interpreted due to the increase of the bandwidths assuming the band centers constant.[34] The present result implies that compression along the *a* axis and/or the *c* axis also plays an important role, however.

The Fermi surfaces are located around $k_b=(1/4)\rho b^*$ (ρ, charge transfer) as a result of the quasi-one-dimensionality and the charge transfer. Since there are small but appreciable interchain interactions, the Fermi surfaces are not completely flat as shown in our previous work.[14] The uniaxial compression causes significant changes in intercolumn coupling and great variations in the Fermi-surface structure are expected. Figure 3 represents Fermi-surface views obtained with GGA for the experimental lattice and those under three kinds of compression. They are produced with the 3D CG software POV-Ray,[35] an enhanced version by Suzuki.[36] It is shown that both the electron and hole surfaces change significantly their shapes and sizes. The LDA results are very similar to the GGA ones except the *a*-compression case. In this case, the LDA result shows small electron and hole pockets around $(k_a,k_c)=(a^*/2,0)$. This difference could be ascribed to the differences in t_{FQ}^a and ν mentioned in the preceding paragraph. For the experimental lattice, the electron surface has a pancakelike shape centered at $(k_a,k_c)=(0,0)$. The hole surface also has a flat shape and its center is at $(k_a,k_c)=(a^*/2,0)$. Under the *a* compression, these surfaces become small pockets in the LDA result while they become thin and tubelike in the GGA one. For the *b* compression, these surfaces are connected along the a^* direction and become open surfaces. The c^* compression makes these surfaces small

TABLE V. Tight-binding parameters evaluated with optimized atomic positions for the experimentally obtained unit cell as well as uniaxially deformed ones.

	Expt. lattice		10% *a*		10% *b*		10% *c**	
	LDA	GGA	LDA	GGA	LDA	GGA	LDA	GGA
t_F^b (meV)	203.	191.	163.	154.	381.	372.	194.	191.
t_Q^b (meV)	−195.	−171.	−221.	−205.	−227.	−200.	−228.	−227.
t_F^c (meV)	4.50	4.43	2.24	2.60	3.90	3.85	15.9	14.6
t_Q^c (meV)	−16.5	−17.5	−27.5	−29.8	−22.0	−21.5	−22.5	−20.7
t_{FQ}^a (meV)	5.75	6.07	18.4	3.83	7.56	9.65	11.1	11.1
ν (meV)	−11.5	−9.35	−7.65	−43.3	0.851	1.17	−3.84	−1.69
ρ (electrons)	0.813	0.768	0.925	0.870	0.825	0.795	0.884	0.863

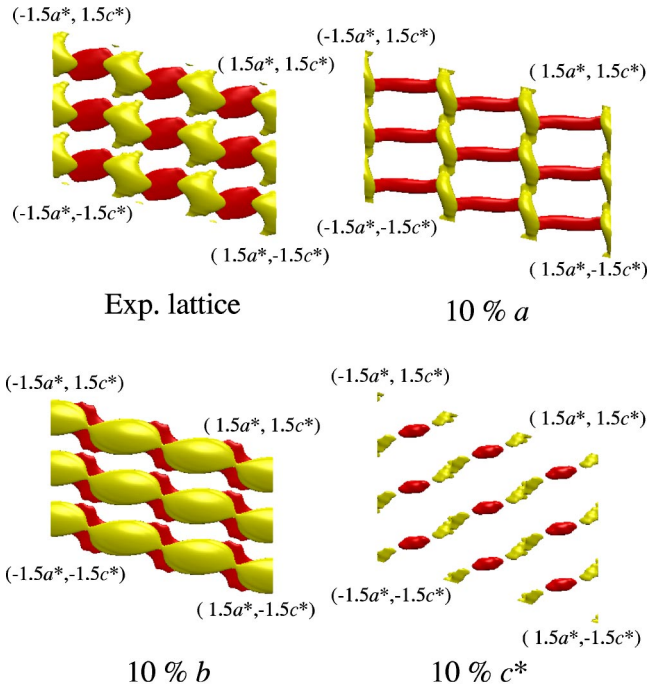

FIG. 3. (Color online) Calculated Fermi surfaces for the experimental unit cell and the compressed cells along the a, b, and c^* axes. Views from the Γ point toward the Y point are shown in the area of $3a^*$ (inclined) $\times 3c^*$ (vertical). Four corners of each figure correspond to $(k_x,k_z)=(-1.5a^*,-1.5c^*)$, $(1.5a^*,-1.5c^*)$, $(-1.5a^*,1.5c^*)$, and $(1.5a^*,1.5c^*)$, respectively. Dark (red for online) ones represent electron surfaces while bright (yellow) ones represent hole surfaces. The GGA results are shown.

pockets. Reflecting the variations of the Fermi surfaces, the density of states (DOS) at the Fermi level changes much. Values are listed in Table VI. These changes in the DOS and in the band anisotropies discussed above could affect transport properties of this material. For example, the b compression would increase quasi-one-dimensionality of the conductivity through the band anisotropy and the Fermi-surface shape. On the other hand, the c compression would reduce the conductivity through the decrease of the DOS at the Fermi level.

TABLE VI. Density of states at the Fermi level for the experimentally obtained unit cell as well as uniaxially deformed ones. Values are given in the unit of electrons/eV/unit cell.

	Expt. lattice	10% a	10% b	10% c^*
LDA	4.56	1.64	4.01	1.87
GGA	5.95	4.64	4.61	1.69

IV. CONCLUSION

We have studied the effects of three different uniaxial compressions on the electronic structure of TTF-TCNQ through *ab initio* plane-wave pseudopotential calculations with the atomic positions determined by the molecular-dynamics technique. This procedure would be promising since experimental determination of the atomic positions under compression is not always possible. The molecular shapes change differently depending on the compression direction. As for the compression along the b axis, the molecules do not change its shape. For the other compressions, there are significant changes in the bond angles but less changes in the bond lengths. The electronic structures represented with the band parameters and the Fermi surfaces have changed significantly and differently. The transport properties of TTF-TCNQ could be affected along with these changes and there is a possibility for tuning them by external pressure.

ACKNOWLEDGMENTS

This work was partly supported by a Grant-in-Aid for Scientific Research on Priority Areas of Molecular Conductors (Grant No. 15073226) from the Ministry of Education, Culture, Sports, Science and Technology, Japan. All the calculations were performed utilizing computing resources at the Tsukuba Advanced Computing Center (TACC) at National Institute of Advanced Industrial Science and Technology (AIST), under Ministry of Economy, Trade and Industry, Japan (METI).

[1] J.P. Ferraris, D.O. Cowan, V. Walatka, Jr., and J.H. Perlstein, J. Am. Chem. Soc. **95**, 948 (1973).
[2] M.J. Cohen, L.B. Coleman, A.F. Garito, and A.J. Heeger, Phys. Rev. B **10**, 1298 (1974).
[3] T.J. Kistenmacher, T.E. Phillips, and D.O. Cowan, Acta Crystallogr., Sect. B: Struct. Crystallogr. Cryst. Chem. **30**, 763 (1974).
[4] R.H. Blessing and P. Coppens, Solid State Commun. **15**, 215 (1974).
[5] S. Kagoshima, T. Ishiguro, and H. Anzai, J. Phys. Soc. Jpn. **41**, 2061 (1976).
[6] S. Megtert, R. Comès, C. Vettier, R. Pynn, and A.F. Garito, Solid State Commun. **31**, 977 (1979).
[7] A.J. Berlinsky and J.F. Carolan, Solid State Commun. **15**, 795 (1974).
[8] F. Herman, D.R. Salahub, and R.P. Messmer, Phys. Rev. B **16**, 2453 (1977).
[9] S. Shitzkovsky, M. Weger, and H. Gutfreund, J. Phys. (France) **39**, 711 (1978).
[10] E.B. Starikov, Solid State Commun. **91**, 45 (1994).
[11] R.V. Kasowski, M.-H. Tsai, S.T. Chui, and J.D. Dow, Phys. Rev. B **46**, 10 017 (1992).
[12] T. Miyazaki, K. Terakura, Y. Morikawa, and T. Yamasaki, Phys. Rev. Lett. **74**, 5104 (1995).
[13] S. Ishibashi and M. Kohyama, J. Low Temp. Phys. **117**, 1753 (1999).

[14] S. Ishibashi and M. Kohyama, Phys. Rev. B **62**, 7839 (2000).
[15] S. Ishibashi, A.A. Manuel, D. Vasumathi, A. Shukla, P. Suortti, M. Kohyama, and K. Bechgaard, J. Phys.: Condens. Matter **11**, 9025 (1999).
[16] S. Ishibashi, A.A. Manuel, L. Hoffmann, and K. Bechgaard, Phys. Rev. B **55**, 2048 (1997).
[17] S. Ishibashi and M. Kohyama, Radiat. Phys. Chem. **58**, 437 (2000).
[18] M. Sing, U. Schwingenschlögl, R. Claessen, P. Blaha, J.M.P. Carmelo, L.M. Martelo, P.D. Sacramento, M. Dressel, and C.S. Jacobsen, Phys. Rev. B **68**, 125111 (2003).
[19] J. Fraxedas, Y.J. Lee, I. Jiménez, R. Gago, R.M. Nieminen, P. Ordejón, and E. Canadell, Phys. Rev. B **68**, 195115 (2003).
[20] S. Kagoshima, R. Kondo, H. Hirai, T. Shibata, Y. Kaga, and M. Maesato, Phys. Status Solidi B **223**, 97 (2001).
[21] D.R. Hamann, M. Schluter, and C. Chiang, Phys. Rev. Lett. **43**, 1494 (1979).
[22] N. Troullier and J.L. Martins, Phys. Rev. B **43**, 1993 (1991).
[23] L. Kleinman and D.M. Bylander, Phys. Rev. Lett. **48**, 1425 (1982).
[24] S.G. Louie, S. Froyen, and M.L. Cohen, Phys. Rev. B **26**, 1738 (1982).
[25] D.M. Ceperley and B.J. Alder, Phys. Rev. Lett. **45**, 566 (1980).
[26] J.P. Perdew and A. Zunger, Phys. Rev. B **23**, 5048 (1981).
[27] J.P. Perdew, K. Burke, and M. Ernzerhof, Phys. Rev. Lett. **77**, 3865 (1996).
[28] M.P. Teter, M.C. Payne, and D.C. Allan, Phys. Rev. B **40**, 12 255 (1989).
[29] D.M. Bylander, L. Kleinman, and S. Lee, Phys. Rev. B **42**, 1394 (1990).
[30] G.P. Kerker, Phys. Rev. B **23**, 3082 (1981).
[31] M. Kohyama, Modell. Simul. Mater. Sci. Eng. **4**, 397 (1996).
[32] C.-L. Fu and K.-M. Ho, Phys. Rev. B **28**, 5480 (1983).
[33] J. Ihm, A. Zunger, and M.L. Cohen, J. Phys. C **12**, 4409 (1979).
[34] T. Tiedje, R.R. Haering, M.H. Jericho, W.A. Roger, and A. Simpson, Solid State Commun. **23**, 713 (1977).
[35] See http://www.povray.org/
[36] R. Suzuki, AIST Today **2–11**, 12 (2002) (ISSN 1346-5805) [in Japanese, a public relations magazine of National Institute of Advanced Industrial Science and Technology (AIST), available at http://www.aist.go.jp/aist_j/aistinfo/aist_today/at_research_main.html].